Proceeding of the IEEE
International Conference on Robotics and Biomimetics
Dali, China, December 2019

Optimal Steering of Stochastic Mobile Robots that Undergo Collisions with their Environment

Zhouyu Lu and Konstantinos Karydis
Department of Electrical and Computer Engineering
University of California, Riverside
900 University Ave., Riverside, CA 92521, USA
{*zlu044, karydis*}*@ucr.edu*

***Abstract*— The paper introduces a state-feedback closed-loop control approach with integrated collision exploitation. We represent the system's kinematics in the form of a drift-diffusion stochastic differential equation, and follow a stochastic switching framework to model the transition between states of free motion and in collision with the environment. We formulate an optimal steering problem and compute the control input related to state feedback. Collisions are found beneficial in terms of increasing task success probability when steering a robot from an initial to a target spatial distribution. In certain cases, collisions may help reduce the control energy for the task when compared to optimal steering with collision avoidance. We provide a mathematical basis to explain this finding, perform several parametric analyses in simulation to validate the theoretical analysis, and conduct realistic physics simulations to quantify the impact of realistic constraints (bounded control input, physical impact of collision, and friction) on control energy and success probability. Further, we validate the proposed approach experimentally with an omni-directional collision-resilient wheeled robot.**

***Index Terms*— Stochastic Control, Optimal Steering, Stochastic Switching Framework**

I. Introduction

As robots increasingly venture outside the protected lab environment and into the real—uncertain—world, guaranteeing collision avoidance becomes an even more challenging task [1], [2]. At the same time, recent advances in material science and mechanical design have helped introduce robots that can safely withstand collisions (e.g., small legged robots with exoskeletons [3], aerial robots with protective cages [4], and soft robots [5]). Taken together, these observations may explain an emerging paradigm shift: *Collisions with the environment could be harnessed instead of being avoided*. In fact, recent works have demonstrated how allowing for collisions can benefit motion planning and control [6], localization [7], and sensing [8]. This present paper focuses on harnessing collisions for robot motion planning and control.

Existing works on collision-based motion planning and control are typically feedforward in nature. For instance, colliding with the environment may increase the probability of success for reaching a target [6], and may improve navigation through confined environments [9], including multi-robot systems [10]. However, controlled mobility (i.e. feedback-based robot navigation) under collisions is critically missing. Introducing feedback strategies alongside existing feedforward approaches would be beneficial. Indeed, while feedforward approaches essentially describe what is the impact of collisions in robot navigation, feedback approaches could help determine *how to best utilize* those collisions.

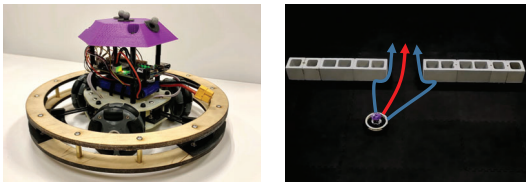

Fig. 1: (Left) The omni-directional collision-resilient wheeled robot we use to validate the theoretical analysis and simulation results. (Right) This paper's case study evaluates the efficacy of a stochastic mobile robot to navigate through a narrow aperture when colliding with its environment (arrows in blue) compared to when navigating directly through the aperture without colliding (arrow in red).

In this paper, we design a feedback motion control strategy for a mobile robotic agent that intentionally collides with the environment. The motion of the agent is considered to be stochastic so as to retain relevance to practical applications where robot motion is affected by uncertainty [11]. To address motion uncertainty, we model the system by a drift-diffusion stochastic differential equation (SDE) [12], [13]. We capture transitions between states of free motion and in collision with the environment via a stochastic switching framework [14], and build on top of recent efforts to include such boundary interactions within an SDE-based modeling framework [15]. The latter work [15] shows that boundary interaction during wall-following has a positive effect on limiting the rate of increase of position uncertainty for the system. However, that approach is developed with a feedforward control design at its core. On the contrary, we consider here a state-feedback closed-loop control approach with integrated collision exploitation.

*We gratefully acknowledge the support of NSF under grant # IIS-1910087 and ONR under grant # N00014-19-1-2264. Any opinions, findings, and conclusions or recommendations expressed in this material are those of the authors and do not necessarily reflect the views of the funding agencies.

978-1-7281-6321-5/19//$31.00 ©2019 IEEE

Once an SDE model is formulated, we seek to compute feedback control gains to steer the system from an initial to a target spatial distribution, *while colliding with the environment*. This problem, different from classical LQG [16], can be formulated as steering optimally the distribution of a diffusion process [17]. Related work [18], [19] addresses the optimal steering problem over a finite horizon with minimum energy, employing semidefinite optimization to calculate appropriate feedback gains under unbounded control inputs. Recent work [20] extends the principle of optimal steering [18], [19] to covariance control and path planning for stochastic systems under chance constraints. However, interactions between the robot and the environment are not accounted for in any of these related efforts. Our work offers a formal framework to account for and exploit collisions.

We first form an optimal steering problem and compute the appropriate state feedback. Since the agent is unaware of potential obstacles between initial and target distributions, we integrate models for boundary interaction on the closed-loop system. Hence, we design a switched optimal steering control method. The developed method is thoroughly tested in Monte-Carlo simulation with point and omni-directional wheeled mobile robots, to evaluate the control energy and task success rates associated with colliding with the environment across a range of different conditions. Furthermore, the approach is validated experimentally with an omni-directional collision-resilient wheeled robot (see Fig. 1).

The main contributions of the paper are as follows:

- We design a stochastic switching framework for feedback motion control of robotic agents undergoing collisions with the environment.
- We study under which conditions colliding with the environment may lead to less control energy to steer from an initial to target spatial distribution.
- We investigate the effect of unbounded and bounded control inputs to the total required control energy and task success rates for reaching a target distribution under point and omni-directional robot kinematics.

Our work is a step forward to enabling controlled mobility of mobile robots that operate under uncertainty. The presented method can also be beneficial to robots that lack sufficient sensing capabilities to detect obstacles and/or ingress-egress points (which are important to real-world applications like disaster response), such as small robots [21].

II. Technical Preliminaries

We first introduce the necessary technical preliminaries on finite-horizon optimal steering, that are later applied to calculate the control input $\mathbf{u}(t)$ of the robotic agent going from an initial to a target distribution within a finite interval.[1]

[1]The material in this section is adapted from the original work on optimal steering [18], [19]. To balance limited space and making the paper self-contained, we cover here only the results that our work directly builds upon. For further details on optimal steering, we refer the reader to [18], [19].

The finite-horizon optimal steering problem [18] of a linear time invariant (LTI) system can be formulated as:

$$\begin{aligned} \underset{\mathbf{u}(t)}{\text{minimize}} \quad & J(\mathbf{u}(t)) = \mathbb{E}\{\int_0^T \mathbf{u}'(t)\mathbf{u}(t)dt\} \ , \\ \text{subject to} \quad & d\mathbf{x}^{\mathbf{u}}(t) = A\mathbf{x}^{\mathbf{u}}(t) + B\mathbf{u}(t) + B_1(t)d\mathbf{w}(t) \\ & \mathbf{x}^{\mathbf{u}}(0) = \mathbf{x}_0 \\ & \mathbf{x}^{\mathbf{u}}(T) = \mathbf{x}_T \ a.s. \ , \end{aligned} \tag{1}$$

where $\mathbf{x}_0$ and $\mathbf{x}_T$ are n-dimensional Gaussian vectors with covariance Σ_0 and Σ_T, respectively. The initial state $\mathbf{x}_0$ is assumed independent of the system's uncertainty $w(t)$, where $\{w(t)|0 \leqslant t \leqslant T\}$ is taken to be the standard p-dimensional Wiener process. Matrices A, B, and B_1 take values in $\mathbb{R}_{n\times n}$, $\mathbb{R}_{n\times m}$, and $\mathbb{R}_{n\times p}$, respectively.

Under the condition that the deterministic subsystem $(A,\ B)$ is controllable, the optimal control input in problem (1) is a linear function of the states [19]:

$$\mathbf{u}(t) = K(t)\mathbf{x}(t),\ t \in [0, T] \ . \tag{2}$$

Without loss of generality let $\mathbb{E}\{\mathbf{x}_0\} = 0$.[2] Consider also $\mathbb{E}\{\mathbf{x}_0\mathbf{x}_0'\} = \Sigma_0$.[3] The state covariance $\Sigma(t) = \mathbb{E}\{\mathbf{x}_t\mathbf{x}_t'\}$ with input (2) satisfies the Lyapunov differential equation

$$\dot{\Sigma}(t) = (A-BK(t))\Sigma(t)+\Sigma(t)(A-BK(t))'+B_1B_1' \ . \tag{3}$$

Let $H(t) = -\Sigma(t)K'(t)$. If $H(t)$ and $K(t)$ are in bijective correspondence (i.e. when $\Sigma(t) > 0$), we can rewrite (3) as

$$\dot{\Sigma}(t) = A\Sigma(t) + \Sigma(t)A' + BH'(t) + H(t)B' + B_1B_1' \ . \tag{4}$$

Given any two positive definite covariance matrices Σ_0 and Σ_T, there is a smooth input $\mathbf{u}(t)$ so that the system satisfies the boundary conditions and $\Sigma(t) > 0$ for all $t \in [0,\ T]$ [18].

To compute the optimal feedback gain, we reformulate the objective function of problem (1) as

$$\begin{aligned} J(\mathbf{u}(t)) = \mathbb{E}\{\int_0^T \mathbf{u}'(t)\mathbf{u}(t)dt\} &= \int_0^T trace(K(t)\Sigma(t)K'(t))dt \\ &= \int_0^T trace(H'(t)\Sigma(t)^{-1}H(t))dt \ , \end{aligned} \tag{5}$$

with constraints $\Sigma(0) = \Sigma_0$ and $\Sigma(T) = \Sigma_T$.

To compute $K(t)$ numerically, we solve a semi-definite program (SDP). The objective function is $\int_0^T trace(Y(t))dt$, with constraints (4) and $\begin{bmatrix} Y(t) & H'(t) \\ H(t) & \Sigma(t) \end{bmatrix} \succcurlyeq 0$.

[2]This condition can be achieved by initially aligning the global and local (body-fixed) coordinate systems.

[3]In practice, pose estimation covariance Σ_0 is determined experimentally.

III. Optimal Steering under Collisions

We design the framework to perform optimal steering for robot behaviors that alternate between free-space motion and collision states. For sake of clarity, the type of collision we consider here includes wall-following. The system collides with a wall and remains in contact with it for some amount of time. Yet, our framework is general and can also handle instantaneous collisions with isolated obstacles.

For concreteness, the task we consider is to go through a narrow aperture (such as a door or a window) without explicit knowledge of the latter's location. We require that the robot 1) has the capacity to infer bearing to the target (e.g., through a compass), and 2) can detect when it reaches the aperture (e.g., through IR range finder).[4]

A. Optimal Steering for Free-space Motion

Under the condition that motion along the x and y body-fixed coordinate axes is uncorrelated, the system model attains the SDE form

$$\begin{bmatrix} dx(t) \\ dy(t) \end{bmatrix} = \mathbf{v}(t)dt + B_{xy}\mathbf{u}(t)dt + \begin{bmatrix} b_{1_x}^2 & 0 \\ 0 & b_{1_y}^2 \end{bmatrix} dw \ , \quad (6)$$

with $B_{xy} = \begin{bmatrix} b_x & 0 \\ 0 & b_y \end{bmatrix}$ and $\mathbf{v}(t) = \begin{bmatrix} v_x(t) \\ v_y(t) \end{bmatrix}$.

The control input is $\mathbf{u}(t) = \begin{bmatrix} u_x(t) & u_y(t) \end{bmatrix}' = \begin{bmatrix} k_x(t)(x - v_x t) & k_y(t)(y - v_y t) \end{bmatrix}'$. This problem is posed in form (1); based on (5), the objective function becomes

$$\begin{aligned} J &= \int_0^T k_x^2(t)\sigma_x(t)dt + \int_0^T k_y^2(t)\sigma_y(t)dt \\ &= \int_0^T h_x^2(t)\sigma_x^{-1}(t)dt + \int_0^T h_y^2(t)\sigma_y^{-1}(t)dt = J_x + J_y \ , \end{aligned}$$

while based on (4) we get

$$\dot{\sigma}_x(t) = 2b_x h_x(t) + b_{1_x}^2, \text{ and } \dot{\sigma}_y(t) = 2b_y h_y(t) + b_{1_y}^2 \ . \quad (7)$$

B. Piece-wise Optimal Steering with Collision Avoidance

To avoid collisions with the wall, entering through the aperture can be modeled as a piece-wise optimal steering problem. That is, we first steer the robot to the middle of the aperture, and from there to the target area. Since the (linear) system kinematics do not change across intervals, (2) can be directly extended to the piece-wise case. In the general case, given target Gaussian distributions in each switching point T_i with covariance Σ_{T_i}, we can compute feedback gains $K_i(t)$ that minimize the control energy at each interval separately. Then, the feedback gain is a piece-wise function of t, i.e.

$$K(t) = \begin{cases} K_1(t) & T_0 \leqslant t \leqslant T_1 \\ K_2(t) & T_1 \leqslant t \leqslant T_2 \\ \vdots & \vdots \\ K_N(t) & T_{N-1} \leqslant t \leqslant T_N \ . \end{cases}$$

C. Integration of Collisions

We apply a stochastic switching framework [15] to model the combined system behavior as it switches between wall-following and free-space motion. When in free space mode, (7) applies with $b_{1_x} = b_{1_x,free}$ and $b_{1_y} = b_{1_y,free}$. When in wall-following mode, the robot maintains a local orientation such that its body-fixed x-axis is parallel to the wall. Diffusion matrix $B_{1_{xy},wall}$ is diagonal, positive definite, and constant with $b_{1_x} = b_{1_x,wall}$ and $b_{1_y} = b_{1_y,wall}$. We assume that $b_{1_x,wall} = b_{1_x,free}$ and $b_{1_y,wall} \leqslant b_{1_y,free}$. That is because the noise along they y direction can be quickly compensated for due to the wall [15]. Then, the whole motion can be formulated as a linear, piece-wise drift-diffusion equation in free-space and wall-following modes.

D. Effect on Control Energy

A potential benefit of colliding with the environment is that it may reduce the required control energy to reach a target distribution, *under certain conditions*. The main reason is that the presence of the wall reduces uncertainty in motion [6], [15] which in turns leads to reduced control energy. In the remainder of this section we offer a mathematical basis explaining why the required control energy might reduce. Section IV evaluates the effect of collisions on control energy when the physical impact of the collision is neglected. Then in Section V we relax several assumptions and test in simulation, while in Section VI we test via physical experiments.

Let $k_x(t)$ and $k_y(t)$ be as in the linear optimal steering in both free motion and wall-following. The initial distribution and end time stay the same too. When colliding with the wall, the control energy in the x direction is

$$\begin{aligned} J_{x,wall} = &\int_0^{T_i} k_x^2(t)\sigma_{x,wall}(t)dt + \int_{T_i}^{T_d} k_x^2(t)\sigma_{x,wall}(t)dt \\ &+ \int_{T_d}^{T} k_x^2(t)\sigma_{x,wall}(t)dt \ , \end{aligned} \quad (8)$$

where T_i and T_d denote the time of impact and disengaging from the wall, respectively.

We can split the control energy required to perform the same task as if there were no obstacles in three parts, according to switching times T_i and T_d. That is, $J_{x,free} = J_1(0 \leq t \leq T_i) + J_2(T_i \leq t \leq T_d) + J_3(T_d \leq t \leq T)$.

[4]These requirements are realistic since a compass and IR sensors can be directly equipped onto mobile robots.

According to noise kinematics (7) and due to the condition $\sigma_{x,free}(0) = \sigma_{x,wall}(0)$, then $\sigma_{x,wall}(t) = \sigma_{x,free}(t)\ t \in [0, T_i]$. Hence $J_1 = \int_0^{T_i} k_x^2(t)\sigma_{x,wall}(t)dt$. Following the same rationale, and assuming that the processes are stationary [18] so that we can time swift J_3 from $t = T_d$ to $t = 0$, we get that $J_3 = \int_{T_d}^{T} k_x^2(t)\sigma_{x,wall}(t)dt$. In wall-following mode the Lyapunov differential equation in x direction is chosen to be

$$\dot{\sigma}_{x,wall}(t) = 2b_x h_x(t) + b_{1_x,wall}^2 - Q(t)\ . \tag{9}$$

$Q(t)$ is added to account for the wall-following effect on $\sigma_x(t)$. We consider $Q(t) \geqslant 0$ since the wall-following motion decreases the rate of diffusion over the x direction [15]. Therefore, we get $\sigma_{x,wall}(t) \leqslant \sigma_{x,free}(t)$. Then

$$\begin{aligned}\int_{T_i}^{T_d} k_x^2(t)\sigma_{x,wall}(t)dt &= \lim_{n\to\infty}\sum_{i=1}^{n} k_x^2(\xi_i)\sigma_{x,wall}(\xi_i)\Delta t \\ &\leqslant \lim_{n\to\infty}\sum_{i=1}^{n} k_x^2(\xi_i)\sigma_{x,free}(\xi_i)\Delta t \\ &= \int_{T_i}^{T_d} k_x^2(t)\sigma_{x,free}(t)dt = J_2\end{aligned}$$

with $\xi_i \in [t_i, t_{i+1})$. Thus, $J_{x,wall} \leq J_{x,free}$.

The same steps apply to the control energy along the y direction. For wall-following when $t \in (T_i, T_d]$, $b_{1_y,wall}^2 \leqslant b_{1_y,free}^2$ and based on the noise kinematics

$$\dot{\sigma}_{y,wall}(t) = 2b_y h_y(t) + b_{1_y,wall}^2\ , \tag{10}$$

we get $\sigma_{y,wall}(t) \leqslant \sigma_{y,free}(t)$ leading to $J_{y,wall} \leqslant J_{y,free}$. Since motions in the x and y directions are assumed independent from each other, $J_{wall} = J_{x,wall} + J_{y,wall} \leq J_{x,free} + J_{y,free} = J_{free}$.

As an immediate consequence, and by the triangle inequality on the system's stochastic process, we get $J_{wall} \leq J_{free} \leq J_{ncol}$, where J_{ncol} denotes the control energy to steer through the aperture without collision.

IV. Simulation with Point Robot

We run simulations to study the effect of boundary interactions when going through an aperture such as a door. In this section we focus on a point robot and conduct an extensive parametric study. In the next section we focus on a omni-directional wheeled robot. The setup is shown in Fig. 2.

The agent begins at randomly selected initial positions (along the X axis of a global frame) at a distance $D_1 = 5\ m$ from the door along the Y global axis. The target distribution has a mean at a distance $D_2 = 5\ m$ from the door along the global Y axis, while its X location is at the midpoint of the door. The length of the door D_d is allowed to vary across different sets of simulations.

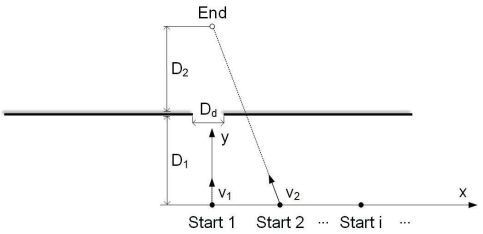

Fig. 2: Simulation study setup.

The following assumptions are made in this case study:

- The thickness of the wall is ignored.
- Friction and collision impact are ignored.
- The robot has some localization capacity so that it can use the location as state feedback.
- The robot has some wall identification capabilities so that it knows when it is in contact with the wall.
- The robot has bearing information to the target and hence can correctly determine along which direction of the wall to move after collision.

Remark 1. *The purpose of this case study is to shed light on the tradeoffs between the various parameters of the problem in the ideal case where physical collision impact is negligible. Later in Section V, that focuses on an omni-directional wheeled robot, we relax the environment assumptions on wall thickness, friction, and collision impact. Further, in Section VI, we validate the theory and simulation experimentally.*

The diagonal elements of diffusion matrix in (6) for free-space motion mode are $b_{x,free} = b_{y,free} = 0.1$. The diffusion coefficients change into $b_{x,wall} = 0.1$, $b_{y,wall} = 0.001$ in wall-following mode.

A. Simulation Procedure

We first formulate an optimal steering problem for a stochastic LTI system over a finite horizon to calculate the state feedback gains k_x and k_y in x and y directions, respectively. In the calculation, we assume that the distributions of initial and final state are Gaussian with covariance

$$\Sigma_0 = \begin{bmatrix}100 & 0\\ 0 & 100\end{bmatrix},\ \Sigma_T = \begin{bmatrix}0.1 & 0\\ 0 & 0.1\end{bmatrix}\ .$$

Then, we consider three types of simulations.

1. Simulate the agent's trajectory as if there were no obstacles. The state feedback gain is calculated from the previous step. The drift is a constant speed $[v_x, v_y]$. Euler-Maruyama method is applied to calculate the position.
2. Simulate the agent's trajectory entering through the door while colliding with the wall. We use the same feedback gain as above. To simulate the door entering behavior:
   - We begin simulating the system in free-space mode.
   - We change to wall-following mode when the agent collides. At that instant, the velocity of the robot is set

to $\frac{s}{T_{end}-t}$; s stands for the remaining distance toward the goal, and t is the time of hitting the wall.
- We change back to free-space mode once the agent reaches the edge of the door. The velocity is updated again as $\frac{s}{T_{end}-t}$, where in this case t updates to the time of disengaging from the wall.

3. Simulate the agent's trajectory entering directly through the door without colliding. This case presupposes that information about the door position is available. We now deal with a piece-wise optimal steering problem. To steer the robot into the door, we set $\sigma_x = \frac{D_d}{3}$ and $\sigma_y = \frac{D_d}{3}$ to avoid collisions. Then, we steer it to the target.

We conduct 1000 trials in each simulation case; final time T_{end} is the same in all cases. To study the effect of final time, we let it vary from 5 sec to 25 sec in increasing 5 sec intervals. We also consider T_{end} at 50 and 100 sec. After the simulations conclude, we compare the control energy required by those three scenarios. Then, we vary other parameters like door width and mean of initial distribution to study how those parameters influence the control energy.

Furthermore, we evaluate the effect of bounded control input. For this purpose we define a target area of success by $\begin{bmatrix} x & y \end{bmatrix} \Sigma_T^{-1} \begin{bmatrix} x & y \end{bmatrix}^\intercal \leqslant 3^2$, and run 1000 trials in each simulation to study the influence of bounded control input.

B. Results — Unbounded Control Input

We first compare the control energy required for the aforementioned three types of simulation. The initial variance is $\sigma_{x,0}^2 = \sigma_{y,0}^2 = 100\ m^2$, the target is set at $(0, 10)\ m$ with desired variance $\sigma_{x,T}^2, \sigma_{y,T}^2 \leq 0.1\ m^2$, the final time $T_{end} = 10\ sec$, and the door length $D_d = 1\ m$. These variables remain the same for all three cases.

Table I and Fig. 3 provide a side-by-side comparison for the three types of simulation. Cases 1a (theoretical calculation) and 1b (simulation) in Table I and Fig. 3a correspond to optimal steering as if there were no obstacles. Case 2 in Table I and Fig. 3b correspond to our framework of optimal steering and wall exploitation. Cases 3a (theoretical calculation) and 3b (simulation) in Table I and Fig. 3c correspond to piece-wise optimal steering to avoid obstacles.

Remark 2. *Although the first scenario cannot be attained in practice (the agent will not reach the target as it will collide), we include it here so as to compare with the other two scenarios which are attainable in practice.*

It can be readily verified that wall exploitation significantly reduces the observed final covariance. At the same time, wall exploitation is shown to reduce the amount of control energy needed to steer the system. This result is in accordance with the mathematical analysis in Section III. When comparing the obstacle-free and piece-wise steering, we observe that the final covariance in the simulations are close to the desired one, and confirm that the control energy observed in simulation is lower than the theoretically-derived.

TABLE I: Endpoint statistics and control energy.

Case	Mean $[m]$	Covariance $[m^2]$	Control energy $[J]$
1a	$(0, 10)$	$\begin{bmatrix} 0.1 & 0 \\ 0 & 0.1 \end{bmatrix}$	18.50
1b	$(0.0210, 9.8153)$	$\begin{bmatrix} 0.1229 & 0.0036 \\ 0.0036 & 0.0558 \end{bmatrix}$	17.03
2	$(0.0016, 9.9140)$	$\begin{bmatrix} 0.0053 & 0 \\ 0 & 0.0181 \end{bmatrix}$	11.42
3a	$(0, 10)$	$\begin{bmatrix} 0.1 & 0 \\ 0 & 0.1 \end{bmatrix}$	36.19
3b	$(-0.0090, 9.8429)$	$\begin{bmatrix} 0.1273 & 0 \\ 0 & 0.0734 \end{bmatrix}$	32.01

Table II demonstrates how the choice of final time affects the control energy. For each case shown in Table II we simulate 1000 realizations. We select $\sigma_{x,0}^2 = \sigma_{y,0}^2 = 100\ m^2$, set the target at $(0, 10)\ m$ with desired target covariance $\sigma_{x,T}^2, \sigma_{y,T}^2 \leq 0.1\ m^2$, and choose $D_d = 1\ m$. These variables remain the same for all seven cases. E_{1a} and E_{1b} denote the energy required for obstacle-free optimal steering in theory and in simulation, respectively. E_2 denotes the energy required for optimal steering with collision exploitation (our proposed approach) in simulation. Finally, E_{3a} and E_{3b} denote the energy required for piece-wise collision-free optimal steering in theory and in simulation, respectively.

TABLE II: Effect of final time on control energy.

$T_{end}\ [sec]$	$E_{1a}\ [J]$	$E_{1b}\ [J]$	$E_2\ [J]$	$E_{3a}\ [J]$	$E_{3b}\ [J]$
5	36.93	34.23	23.84	72.31	69.43
10	18.50	17.03	11.42	36.19	32.01
15	12.43	11.07	8.69	24.43	20.95
20	9.37	8.12	6.21	18.45	16.21
25	7.52	6.30	5.25	14.82	12.57
50	3.90	3.21	2.66	7.51	7.20
100	1.94	1.70	1.17	3.81	3.65

We observe that no matter the choice of final time, the control energy when exploiting collisions remains significantly lower than the control energy for obstacle-free and piece-wise collision-free optimal steering. While the absolute values drop as we increase the final time (which is expected), our method still serves as a lower bound to the required control energy. Figure 4 shows this trend. Simulation findings are in agreement with our theoretical analysis.

An interesting observation is that the energy savings (P_i, $i \in \{1a, 1b, 2, 3a, 3b\}$ expressed as a percentage) appear to be less dependent on final time. As depicted in Table III, the average control energy savings are approximately 32% and 65% when compared to the theoretical values of obstacle-free and piece-wise collision-free optimal steering, respectively. The respective values obtained through simulation are more

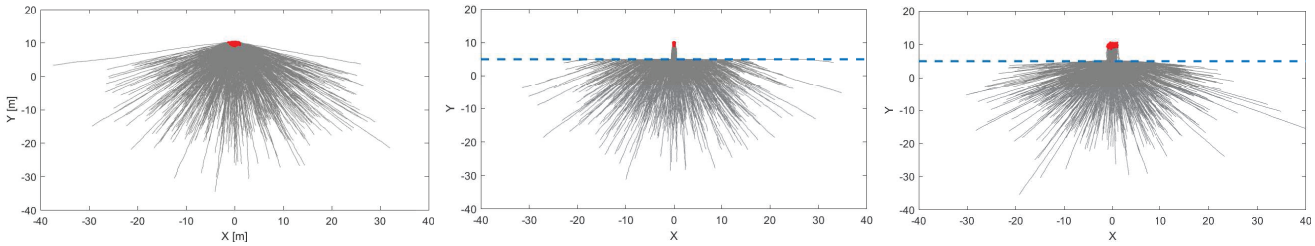

(a) Optimal steering without obstacles (b) Wall exploitation (c) Piece-wise optimal steering with obstacles

Fig. 3: Simulated runs for the three conditions we consider here. In each case we demonstrate 1000 realizations. It can be seen that the final covariance (shown in red color) is significantly lower when we exploit collisions.

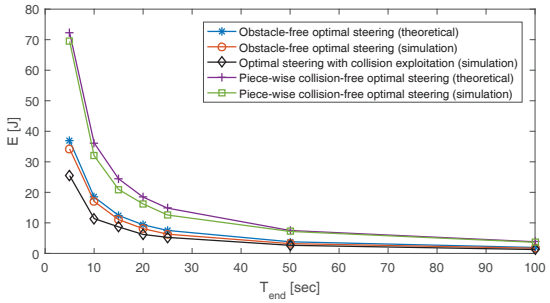

Fig. 4: Control energy of the different methods as final time varies.

TABLE III: Effect of final time on energy savings.

T_{end} $[sec]$	P_{1a} [%]	P_{1b} [%]	P_{3a} [%]	P_{3b} [%]
5	−31.00	−25.55	−64.76	−63.30
10	−37.30	−32.97	−68.46	−64.34
15	−30.11	−21.55	−64.44	−58.54
20	−33.66	−23.47	−66.32	−61.68
25	−30.22	−16.74	−64.60	−58.26
50	−30.24	−17.18	−64.61	−63.09
100	−34.25	−24.85	−66.50	−64.95
$MEAN$	−32.40	−23.19	−65.67	−62.02
STD	2.55	5.13	1.39	2.48

volatile (notice the higher standard deviations); however, the variations seem independent of the final time.

We then examine the effect of the door width on control energy. In this case we consider our approach and the piece-wise collision-free optimal steering. For each case shown in Table IV, we simulate 1000 realizations. Initial and target spatial distributions are as in the previous case study, while $T_{end} = 10$; these variables stay constant for all seven cases.

The control energy required by our proposed approach that harnesses collisions is the lowest for all tested door widths (see Fig. 5). We observe that as the door width increases, the energy savings of our approach decrease and appear to regulate to approximately 19% and 14% when compared to piece-wise collision-free optimal steering in theory and in simulation, respectively. This is due to two reasons. First, as the door width increases, it is possible to find less energy-demanding optimal controls to navigate through the aperture without colliding. Second, as the wall surface decreases, uncertainty-reducing interactions with the walls become less, thus raising the control energy of our approach.

Further, we investigate the effect of varying the mean of the initial position along the X global axis on control energy. The initial covariance remains at $\sigma^2_{x,0} = \sigma^2_{y,0} = 100\ m^2$. The final time remains $T_{end} = 10$, the desired target covariance $\sigma^2_{x,T}, \sigma^2_{y,T} \leq 0.1\ m^2$, and the door width is kept at $D_d = 1\ m$. We compare our approach with piece-wise collision-free optimal steering in simulation. We collect 1000 realizations for each case shown in Table V.

TABLE IV: Effect of door width on control energy and savings.

D_d $[m]$	E_2 $[J]$	E_{3a} $[J]$	$E_{3b}[J]$	P_{3a} [%]	P_{3b}[%]
1	11.42	36.19	32.01	−68.46	−64.34
2	12.76	33.97	30.72	−62.50	−58.46
3	13.71	31.92	29.88	−57.04	−54.11
5	14.70	28.07	25.28	−47.64	−41.84
10	16.07	21.21	18.74	−24.24	−14.27
15	16.36	18.53	16.72	−11.75	−2.20
20	16.16	20.14	18.81	−19.78	−14.14

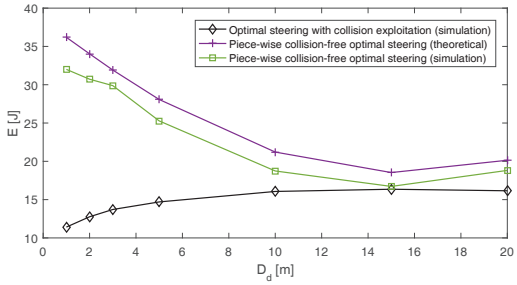

Fig. 5: Control energy of the different methods as door width varies.

TABLE V: Effect of initial position on control energy

$\mu_{x,0}$ $[m]$	E_2 $[J]$	E_{3b} $[J]$
0	11.42	32.01
5	12.95	33.33
10	13.71	32.03
15	13.26	34.20
20	14.77	31.86

Results reveal two key insights. First, the control energy of our approach increases as we get further away from the door. The reason is that the relative portion of interacting with wall over free-space motion decreases, and is in agreement

with the effect of increasing door width. Changes are small since the initial covariance is comparatively high (cf. Fig. 3). Second, the control energy of piece-wise optimal steering remains very close to the theoretically-derived value of $32.03\ J$. This is because the initial condition only influences the drift part, and hence optimal-steering should be agnostic to the expectation of the initial point.

V. Simulation with Omni-directional Robot

In the previous section we showed the validity of the theoretical analysis suggesting that collisions can reduce uncertainty, and they might decrease the required control energy to steer from an initial to a target distribution. The purpose of this section is twofold: First, to show that the proposed method applies to more realistic robots with velocity control bounds. Second, to relax some key assumptions, mainly the one where the physical impact of collision was neglected.

We consider a virtual omni-directional wheeled robot of mass $0.08\ kg$ and dimensions $0.08\ m \times 0.08\ m \times 0.019\ m$, with kinematics as in (6). We simulate the robot via ROS and Gazebo based on [22]. The wall has $0.05\ m$ thickness. We further test the effect of friction between the robot and the wall; namely we pick three friction coefficients: 0, 0.6, and 1. We consider two distinct velocity bounds: $v_{bound} = 2\ m/s$ and $v_{bound} = 5\ m/s$. We compare the proposed optimal steering with collision exploitation to piece-wise collision-free optimal steering. In total we have 12 distinct sub-case studies; for each we simulate 100 realizations. We set $D_1 = D_2 = 5\ m$, and $D_d = 1\ m$. The initial variance is $\sigma^2_{x,0} = \sigma^2_{y,0} = 100\ m^2$, the target is set at $(0, 10)\ m$ with desired variance $\sigma^2_{x,T}, \sigma^2_{y,T} \leq 0.1\ m^2$. Final time T is calculated by $T = \frac{1}{v_{bound}}\sqrt{(3\sigma_{x,T})^2 + (3\sigma_{y,T} + D_1 + D_2)^2}$ so as to force test cases to stay within a given velocity bound. Hence, $v_{bound} = 2\ m/s$ and $v_{bound} = 5\ m/s$ lead to final times of $T = 25\ s$ and $T = 10\ s$, respectively.

To evaluate the 12 conditions we calculate the task success probability P_{omni} over 100 realizations, and the mean control energy of the successful realizations by $E_c = \int_0^T \frac{1}{2} m \mathbf{v}_c^\top \mathbf{v}_c$, where $\mathbf{v}_c$ is calculated by the sum of drift velocity and optimal steering control input of the robot. Table VI contains the task success probabilities and required control energy.

We can make the following observations. First, it appears that optimal steering with collision exploitation can lead to higher task success probabilities than piece-wise collision-free optimal steering at comparative control costs at low speeds. Friction with the wall appears to play a secondary role in terms of control energy, but it may decrease task success probabilities, at low speeds. At higher speeds, both methodologies are negatively impacted, both in terms of success probabilities and required control energy to successfully achieve the task. Optimal steering with collision exploitation is more significantly impacted by speed. Both evaluation metrics are found to be lower than those of piece-wise collision-free optimal steering. In the simulation, we observe that the robot tends to flip over much more frequently as the speed increases; especially when the robot collides with one of its omni-wheels. To mitigate part of this effect, we expect that a protective round bumper which can redirect the restitution force [23], [24] can be beneficial; we test the hypothesis experimentally in the section that follows. Finally, we seek to investigate at what speed bounds collisions may no longer beneficial in terms of improving tasks success rates. As per the current simulated setup, we identify that $v^\dagger_{bound} = 2.5\ m/s$ appears to be the switching behavior bound. To determine this bound, we performed 20 simulation runs at $0.5\ m/s$ velocity intervals and identify the velocity bound where success probability of piece-wise collision-free optimal steering exceeds the one for optimal-steering with collision exploitation.

TABLE VI: Task success probability and required control energy for an omni-directional robot.

Case	Metric	Wall friction coefficient		
		0	0.6	1
Collision exploitation $v_{bound} = 2\ m/s$	$E_c[J]$	1.81	1.49	1.87
	$P_{omni}[\%]$	93	92	87
Piece-wise collision-free $v_{bound} = 2\ m/s$	$E_c[J]$	1.72	1.74	1.62
	$P_{omni}[\%]$	85	80	78
Collision exploitation $v_{bound} = 5\ m/s$	$E_c[J]$	4.15	4.26	3.50
	$P_{omni}[\%]$	31	24	33
Piece-wise collision-free $v_{bound} = 5\ m/s$	$E_c[J]$	3.62	3.01	3.20
	$P_{omni}[\%]$	53	56	44

VI. Experimental Validation

In this section, we test the control strategies in section V on an omni-directional robot equipped with a reflection ring [23] that we build in house. The robot has a mass of $0.639\ kg$ and a body diameter of $0.22\ m$. We consider two distinct velocity bounds: $v_{bound} = 0.5\ m/s$ and $v_{bound} = 1\ m/s$. Robot position data are captured using a 12-camera VICON motion capture system. In the physical experiment, we set $D_1 = D_2 = 4\ m$ and $D_d = 0.2\ m$. The initial variance is $\sigma^2_{x,0} = \sigma^2_{y,0} = 1\ m^2$. For each case shown in Table VII, we perform 10 trials in the physical environment.

TABLE VII: Task success probability and required control energy for an omni-directional robot in experiments.

Case	Metric	Result
Collision exploitation $v_{bound} = 0.5\ m/s$	$E_c[J]$	0.3214
	$P_{omni}[\%]$	100
Piece-wise collision-free $v_{bound} = 0.5\ m/s$	$E_c[J]$	0.3102
	$P_{omni}[\%]$	100
Collision exploitation $v_{bound} = 1\ m/s$	$E_c[J]$	0.9467
	$P_{omni}[\%]$	100
Piece-wise collision-free $v_{bound} = 1\ m/s$	$E_c[J]$	0.6822
	$P_{omni}[\%]$	70

The physical experiment validates the results presented in Section V. With the application of the collision protection

device, the success rate of robot reaching the goal area is improved when applying collision exploitation as the velocity increases. Further, we notice that as the velocity increases, the task success probabilities remain high, although at higher required control energy.

VII. Conclusions

We design a switched optimal steering method for stochastic systems, evaluate it via extensive simulation with point and omni-directional robots, and validate it experimentally with an omni-directional collision-resilient wheeled robot built in house. Our framework optimally switches between states of free-space motion and interaction with obstacles (such as wall-following), so as to enable controlled mobility under uncertainty with high task success probability. Task success probability, as well as the required control energy of our proposed method of optimal steering with collision exploitation, are thoroughly compared to piece-wise collision-free optimal steering. We show the existence of solutions to the piece-wise optimal steering problem, and provide a mathematical basis that might explain potential reduction of required control energy to steer the robot through a narrow aperture while colliding.

Extensive simulation results validate the theoretical concepts. In the first set of simulations, we consider point robot kinematics, and make certain simplifying conditions, with an eye to evaluating the basic underlying theory. The proposed approach might reduce control energy relative to optimal steering as if there were no obstacles and piece-wise collision-free optimal steering. We further study the effect of key variables on control energy; our method can yield energetically efficient solution across variations.

The second set of simulations moves one step closer to applying the derived theoretical tools in practice, by relaxing several key assumptions. Specifically, we consider omni-directional robot kinematics with bounded control input, and account for the physical impact of collisions and friction via realistic physics simulation. Results show that collisions can be exploited at lower speeds (up to $2 - 2.5\ m/s$) in the sense of increased task success probability over piece-wise collision-free optimal steering with similar control energy. Furthermore, the results of the second set of simulations are validated via physical experimentation.

The proposed approach is evaluated on ingress/egress through narrow apertures such as a window or door, without explicit knowledge of the latter's location relative to the wall. This can benefit applications like disaster response with (small) robots that may lack sufficient sensing and computing capacity to determine ingress/egress points and to localize, but may instead withstand collisions with the environment.

References

[1] M. Hoy, A. S. Matveev, and A. V. Savkin, "Algorithms for collision-free navigation of mobile robots in complex cluttered environments: a survey," *Robotica*, vol. 33, no. 3, pp. 463–497, 2015.

[2] S. Campbell, W. Naeem, and G. W. Irwin, "A review on improving the autonomy of unmanned surface vehicles through intelligent collision avoidance manoeuvres," *Annual Reviews in Control*, vol. 36, no. 2, pp. 267–283, 2012.

[3] D. W. Haldane, C. S. Casarez, J. T. Karras, J. Lee, C. Li, A. O. Pullin, E. W. Schaler, D. Yun, H. Ota, A. Javey *et al.*, "Integrated manufacture of exoskeletons and sensing structures for folded millirobots," *Journal of Mechanisms and Robotics*, vol. 7, no. 2, p. 021011, 2015.

[4] A. Briod, P. Kornatowski, J.-C. Zufferey, and D. Floreano, "A collision-resilient flying robot," *Journal of Field Robotics*, vol. 31, no. 4, pp. 496–509, 2014.

[5] D. Rus and M. T. Tolley, "Design, fabrication and control of soft robots," *Nature*, vol. 521, no. 7553, p. 467, 2015.

[6] K. Karydis, D. Zarrouk, I. Poulakakis, R. S. Fearing, and H. G. Tanner, "Planning with the star (s)," in *IEEE/RSJ International Conference on Intelligent Robots and Systems (IROS)*, 2014, pp. 3033–3038.

[7] S. Mayya, P. Pierpaoli, G. Nair, and M. Egerstedt, "Collisions as information sources in densely packed multi-robot systems under mean-field approximations," in *Robotics: Science and Systems*, 2017.

[8] T. Schmickl, R. Thenius, C. Moeslinger, G. Radspieler, S. Kernbach, M. Szymanski, and K. Crailsheim, "Get in touch: cooperative decision making based on robot-to-robot collisions," *Autonomous Agents and Multi-Agent Systems*, vol. 18, no. 1, pp. 133–155, 2009.

[9] N. S. Rao, S. Kareti, W. Shi, and S. S. Iyengar, "Robot navigation in unknown terrains: Introductory survey of non-heuristic algorithms," Oak Ridge National Lab, technical report ORNL/TM-12410, 1993.

[10] Y. Mulgaonkar, A. Makineni, L. Guerrero-Bonilla, and V. Kumar, "Robust aerial robot swarms without collision avoidance," *IEEE Robotics and Automation Letters*, vol. 3, no. 1, pp. 596–603, 2018.

[11] K. Karydis, I. Poulakakis, J. Sun, and H. G. Tanner, "Probabilistically valid stochastic extensions of deterministic models for systems with uncertainty," *The International Journal of Robotics Research*, vol. 34, no. 10, pp. 1278–1295, 2015.

[12] S. K. Shah, C. D. Pahlajani, and H. G. Tanner, "Probability of success in stochastic robot navigation with state feedback," in *IEEE/RSJ International Conference on Intelligent Robots and Systems (IROS)*, 2011, pp. 3911–3916.

[13] P. Reverdy, B. D. Ilhan, and D. E. Koditschek, "A drift-diffusion model for robotic obstacle avoidance," in *IEEE/RSJ International Conference on Intelligent Robots and Systems (IROS)*, 2015, pp. 6113–6120.

[14] H. Lin, P. J. Antsaklis *et al.*, "Hybrid dynamical systems: An introduction to control and verification," *Foundations and Trends in Systems and Control*, vol. 1, no. 1, pp. 1–172, 2014.

[15] A. Stager and H. G. Tanner, "Stochastic behavior of robots that navigate by interacting with their environment," in *IEEE 55th Conference on Decision and Control (CDC)*, 2016, pp. 6871–6876.

[16] W. H. Fleming and R. W. Rishel, *Deterministic and stochastic optimal control*. Springer Science & Business Media, 2012, vol. 1.

[17] R. Filliger and M.-O. Hongler, "Relative entropy and efficiency measure for diffusion-mediated transport processes," *Journal of Physics A: Mathematical and General*, vol. 38, no. 6, p. 1247, 2005.

[18] Y. Chen, T. T. Georgiou, and M. Pavon, "Optimal steering of a linear stochastic system to a final probability distribution, part i." *IEEE Trans. on Automatic Control*, vol. 61, no. 5, pp. 1158–1169, 2016.

[19] ——, "Optimal steering of a linear stochastic system to a final probability distribution, part ii," *IEEE Trans. on Automatic Control*, vol. 61, no. 5, pp. 1170–1180, 2016.

[20] K. Okamoto, M. Goldshtein, and P. Tsiotras, "Optimal covariance control for stochastic systems under chance constraints," *IEEE Control Systems Letters*, vol. 2, no. 2, pp. 266–271, 2018.

[21] K. Karydis and M. A. Hsieh, "Uncertainty quantification for small robots using principal orthogonal decomposition," in *International Symposium on Experimental Robotics*. Springer, 2016, pp. 33–42.

[22] G. A. Ritter. (2016) Openbase. Accessed on March 1, 2019. [Online]. Available: https://github.com/GuiRitter/OpenBase

[23] A. Stager and H. G. Tanner, "Mathematical models for physical interactions of robots in planar environments," in *International Symposium on Experimental Robotics*. Springer, 2018, in press.

[24] ——, "Composition of local potential functions with reflection," in *2019 International Conference on Robotics and Automation (ICRA)*. IEEE, 2019, pp. 5558–5564.